Photoinduced β-Hydrogen Elimination and Radical Formation with $CpW(CO)_3(CH_2CH_3)$: Ultrafast IR and DFT Studies

Elizabeth A. Glascoe,[⊥] Matthias F. Kling,[†] Jennifer E. Shanoski, Robert A. DiStasio, Jr., Christine K. Payne,[§] Benjamin V. Mork,[‖] T. Don Tilley, and Charles B. Harris*

Department of Chemistry, University of California, and Chemical Sciences Division, Lawrence Berkeley National Laboratory, Berkeley, California 94720

Received May 23, 2006

The initial steps of β-hydrogen elimination from the complex $CpW(CO)_3(CH_2CH_3)$ were studied using ultrafast infrared and step-scan FTIR spectroscopy combined with density functional theory calculations. The reaction was initiated by a pulse of UV light at 266 nm and followed with infrared light on the femto- to microsecond timescale, allowing for the identification and kinetic characterization of transients. In the process of β-H elimination, the primary photoproduct was found to be an α-H stabilized complex and the dynamics of the elusive species *cis*-$CpW(CO)_3(H)(CH_2CH_2)$ were resolved, allowing for a full kinetic and thermodynamic analysis of the reaction. In a side reaction, $CpW(CO)_3^{\bullet}$ is formed via ethyl ligand dissociation; the measured formation rate indicates that the complex forms from a vibrationally excited parent complex. Density functional theory calculations of all relevant transient intermediates and transition states involved in β-H elimination of $CpW(CO)_3(CH_2CH_3)$ are presented. These calculations show two principle mechanisms of β-H elimination, which are discussed in the context of the experimental data.

I. Introduction

The process of β-hydrogen (β-H) elimination is one of the most ubiquitous reactions in homogeneous catalysis.[1−6] It is considered to be the major decomposition pathway for late-transition-metal alkyl catalysts[4−6] and the termination reaction in olefin polymerization.[7] A detailed understanding of the mechanistic pathways of β-H elimination addresses a range of fundamental and practical questions.[2] Despite extensive studies of prototypical group 6 and 8 metal alkyl complexes,[8−15] many questions remain concerning the details of β-H elimination in ambient-temperature solutions, due to their unusually high reactivity.

The principal reaction pathway in the photochemistry of $CpW(CO)_3(CH_2CH_3)$ (**A**), which is based on previous studies,[12−14] is summarized in Figure 1. An unstable 16-electron intermediate (**B**) is generated by the UV photoinduced loss of a single carbonyl. It is believed that species **B** coordinates a solvent molecule from the surrounding bath, forming species **C**.[13] This solvent molecule (L) can act either as a "token ligand" that can easily dissociate or as a stable ligand, preventing further β-H elimination (not shown in Figure 1).[13] It may be possible for **B** to self-solvate and immediately form the bridged hydride intermediate $CpW(CO)_2(\mu\text{-H-}C_2H_4)$ (**D**) on the ultrafast time scale; however, no study has had the time resolution and high spectral resolution to explore this possibility. Previous work has shown that **D** forms, presumably from **C**, on the microsecond time scale.[13]

A cis isomer of the metal hydride, *cis*-$CpW(CO)_2(H)(C_2H_4)$ (**E**), was identified as the first product of β-H elimination;[10−13] however, the small signal and short lifetime of **E** has made the collection of kinetic data for this peak impossible in previous studies.[13] In the final, rate-limiting, step of the reaction the hydride moves from a cis to a trans position relative to the alkyl ligand, forming *trans*-$CpW(CO)_2(H)(C_2H_4)$ (**F**).[12] The decay of

* To whom correspondence should be addressed. E-mail: cbharris@berkeley.edu.

[⊥] Present address: Lawrence Livermore National Laboratory, 7000 East Ave. L-268, Livermore, CA 94550.

[†] Present address: Max-Planck-Institute for Quantum Optics, Hans-Kopfermann-Strasse 1, 85748 Garching, Germany.

[§] Present address: School of Chemistry and Biochemistry, Georgia Institute of Technology, 770 State Street, Atlanta, GA 30332.

[‖] Present address: Regenesis Bioremediation Products, 1011 Calle Sombra, San Clemente, CA 92673.

(1) (a) van der Boom, M. E.; Higgitt, C. L.; Milstein, D. *Organometallics* **1999**, *18*, 2413. (b) Cundari, T. R.; Taylor, C. D. *Organometallics* **2003**, *22*, 4047. (c) Zhao, J.; Hesslink, H.; Hartwig, J. F. *J. Am. Chem. Soc.* **2001**, *123*, 7220. (d) Kogut, E.; Zeller, A.; Warren, T. H.; Strassner, T. *J. Am. Chem. Soc.* **2004**, *126*, 11984. (e) Wadepohl, H.; Kohl, U.; Bittner, M.; Köppel, H. *Organometallics* **2005**, *24*, 2097.

(2) Mehrkhodavandi, P.; Schrock, R. R. *J. Am. Chem. Soc.* **2001**, *123*, 10746.

(3) Huang, X.; Zhu, J.; Lin, Z. *Organometallics* **2004**, *23*, 4154.

(4) Crabtree, R. H. *The Organometallic Chemistry of the Transition Metals*; Wiley: New York, 2001.

(5) Niu, S.; Hall, M. B. *Chem. Rev.* **2000**, *100*, 353.

(6) Cross, R. J. *The Chemistry of the Metal-Carbon Bond*; Wiley: New York, 1985.

(7) Bhaduri, S.; Mukesh, D. *Homogeneous Catalysis: Mechanisms and Industrial Applications*; Wiley: New York, 2000.

(8) (a) Mahmoud, K. A.; Narayanaswamy, R.; Rest, A. J. *J. Chem. Soc., Dalton Trans.* **1981**, 2199. (b) Mahmoud, K. A.; Rest, A. J.; Alt, H. G. *J. Chem. Soc., Dalton Trans.* **1983**, 1011. (c) Alt, H. G.; Eichner, M. E. *Angew. Chem., Int. Ed.* **1982**, *21*, 78. (d) Alt, H. G.; Eichner, M. E. *Angew. Chem., Int. Ed.* **1982**, *21*, 205.

(9) Tyler, D. R. *Inorg. Chem.* **1981**, *20*, 2257.

(10) Hooker, R. H.; Rest, A. J. *J. Chem. Soc., Dalton Trans.* **1984**, 761.

(11) Mahmoud, K. A.; Rest, A. J.; Alt, H. G.; Eichner, M. E.; Jansen, B. M. *J. Chem. Soc., Dalton Trans.* **1984**, 175.

(12) Kazlauskas, R. J.; Wrighton, M. S. *J. Am. Chem. Soc.* **1982**, *104*, 6005.

(13) Johnson, F. P. A.; Gordon, C. M.; Hodges, P. M.; Poliakoff, M.; Turner, J. J. *J. Chem. Soc., Dalton Trans.* **1991**, 833.

(14) Yang, G. K.; Peters, K. S.; Vaida, V. *J. Am. Chem. Soc.* **1986**, *108*, 2511.

(15) Virrels, I. G.; George, M. W.; Johnson, F. P. A.; Turner, J. J.; Westwell, J. R. *Organometallics* **1995**, *14*, 5203.

10.1021/om060455i CCC: $37.00 © 2007 American Chemical Society
Publication on Web 02/15/2007

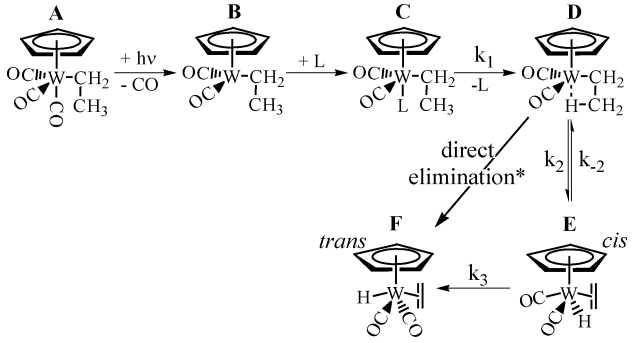

Figure 1. Proposed mechanism for the β-H elimination with CpW(CO)$_3$(CH$_2$CH$_3$) (L = coordinating solvent). Direct elimination was suggested as a mechanism but not investigated in detail in earlier studies.

D and the growth of **F** have been found to be kinetically correlated and best explained by an equilibrium between **D** and **E**.[13]

Figure 1 also displays a direct β-H elimination channel, in which **D** is converted directly into **F**. As direct β-H elimination could occur very rapidly, resulting in the very efficient termination of an olefin polymerization process, it is important to learn whether this reaction is able to occur, even as a minor pathway. A previous study has addressed this question and established that direct elimination does not occur on the nanosecond to microsecond time scale and is not the major pathway to formation of **F**.[12] However, no study investigated this reaction with ultrafast time-resolved infrared spectroscopy. It may be possible for species **D** to form directly from **B** on the ultrafast time scale[16] and subsequently undergo direct elimination to form **F**.

In a side reaction (not shown in Figure 1), the formation of the radical CpW(CO)$_3^\bullet$ is investigated. Previous studies indicate that the radical forms via photodissociation of a methyl group in CpW(CO)$_3$(CH$_3$).[9,15] One would expect a radical to form via the same mechanism when **A** is used, yet no study has documented the formation of the radical species after photoexcitation of **A**.[12,13]

It is clear that the basic mechanism for β-H elimination from **A** has been determined; however, there are a number of important questions that remain, despite previous investigations. What occurs after carbonyl photodissociation? Does **B** coordinate a solvent molecule or rapidly form **D**? What are the dynamics of **E** and are those dynamics consistent with the accepted mechanism? What is preventing direct elimination (**D** → **F**) from happening? Is direct elimination able to occur on the ultrafast time scale? Finally, does a radical species form via photoinduced loss of the ethyl group, and if so, what is the formation and decay mechanism?

In our approach, we used ultrafast time-resolved infrared and step-scan FTIR spectroscopy and density functional theory (DFT) to answer the remaining questions in the photochemistry of **A** and gain a more complete understanding of β-H elimination processes and concurrent photochemistry. The chemistry illustrated for this molecule is representative of a large group of transition-metal alkyl complexes in which the metal, alkyl chain length, and spectator ligands vary.[4,6] The reaction was initiated by a pulse of UV light at 266 nm and followed in the IR on a femto- to microsecond time scale, allowing for the identification and kinetic characterization of important species in the β-H elimination reaction and the radical side reaction. DFT calculations have been used to elucidate the structures and energetics of the intermediates involved, allowing for a comprehensive picture of the photochemistry of **A**.

The results of our studies are discussed in section III. Our DFT results identified multiple isomers of species **B**−**E** and two different mechanisms for β-H elimination: a low-energy pathway in which a carbonyl located cis to the alkyl group is dissociated and a high-energy pathway in which the carbonyl located trans to the alkyl ligand is dissociated. The low-energy, cis-CO loss pathway matches experimental results; the high-energy, trans-CO loss species is able to rearrange, over a couple of small barriers, to the bridged hydride observed in the cis-CO loss pathway. The calculations indicate that direct elimination is not possible and an isomer of species **E** must always form prior to **F**.

Our ultrafast results demonstrate that the first species formed after photodissociation of a carbonyl is most likely the cis isomer of **B** rather than the solvated species **C**. Species **B** rearranges to one of the **D** isomers with a slightly faster rate than previous studies indicated. Our step-scan studies were sensitive enough to resolve the kinetics of one of the isomers of **E**, allowing a full analysis of the barrier heights for the reactions **D** ↔ **E** → **F**. Species **F** is not observed before the microsecond time frame, indicating that direct elimination does not occur in our experiments. Finally, our ultrafast results clearly indicate that the radical species forms, originating from an excited ground state molecule, and subsequently decays on a microsecond time scale.

II. Methods

A. Samples. Spectroscopic grade *n*-hexane and anhydrous ethanol were purchased from Sigma-Aldrich and used without further purification. The starting material, **A**, was prepared by reaction of Na[CpW(CO)$_3$] with ICH$_2$CH$_3$ in THF.[17] Dilute solutions (1−2 mM) were prepared under N$_2$, and all experiments were performed under argon.

B. Femtosecond Infrared Spectroscopy. The experimental apparatus has been described in detail elsewhere.[18] In brief, the setup consists of a Ti:sapphire regenerative amplifier (Spectra-Physics, Spitfire) seeded by a Ti:sapphire oscillator (SpectraPhysics, Tsunami) to produce a 1 kHz pulse train of 100 fs pulses centered at 800 nm with an average pulse power of 0.9 mJ. The output of this system was split and used for both harmonic generation of 266 (0.6 μJ at the sample) pump pulses and to pump a home-built optical parametric amplifier (OPA) able to deliver mid-IR probe pulses tunable from 3 to 6 μm with a spectral width of ca. 200 cm^{-1} and a pulse duration of approximately 100 fs. A computer-controlled translation stage (Klinger) allows for variable time delays up to 800 ps between pump and probe pulses.

The sample was flowed using a mechanical pump through a stainless steel cell (Harrick Scientific) fitted with 1.5 mm thick MgF$_2$ windows. The optical path length was 150 μm, and sample concentrations were adjusted so that the optical density (OD) of the sample at 266 nm was ca. 1. Reference and signal IR beams were sent along a parallel path through a computer-controlled spectrograph (Acton Research Corp., SpectraPro-150) and detected by a 2 × 32 element MCT-array IR detector (InfraRed Associates, Inc.) and a high-speed signal acquisition system and data acquisition software (Infrared Systems Development Corp.) with a resolution of ca. 3 cm^{-1}. In the ultrafast hexane experiments, reference and signal infrared beams were sent through a monochromator (CVI, Digikrom 240) with a spectral resolution of ca. 4 cm^{-1} at a slit width of 400 μm and detected by single-element MCT IR detectors (Electro-Optical Systems). Collected signals were typically normal-

(16) Yeston, J. S.; Tung, T. T.; Burkey, T. J.; Heilweil, E. J. *J. Phys. Chem. B* **2004**, *108*, 4582.
(17) Piper, T. S.; Wilkenson, G. *J. Inorg. Nucl. Chem.* **1956**, *3*, 104.
(18) Shanoski, J. E.; Payne, C. K.; Kling, M. F.; Glascoe, E. A.; Harris, C. B. *Organometallics* **2005**, *24*, 1852.

ized over 1000 laser shots to account for shot-to-shot fluctuations of the laser. Differences in optical density (ΔOD) as small as 5×10^{-5} were observable in the experiments after only 10−15 s of data collection.

C. Nanosecond and Microsecond Step-Scan FTIR Spectroscopy. The experimental setup of the step-scan apparatus has been described in detail elsewhere.[19] For experiments in the 1700−2100 cm^{-1} region with a spectral resolution of ca. 4 cm^{-1}, a KMPV8-1-J2 HgCdTe PV detector (fwhm, 37 ns; RC decay of AC amplifier, 1.4 ms) was employed. AC-coupled and DC-coupled interferometric signals were simultaneously acquired by a 40 MHz, 12 bit digitizer (Model PAD 1232). Samples were photolyzed with 25 ns pulses of the fourth harmonic of a Nd:YAG laser (DCR2A, GCR-3 optics) at 266 nm. Photolysis light was aligned in a nearly collinear geometry (10°) with the infrared beam. To prevent scattered 266 nm light from reaching interferometer and detector optics, AR-coated Ge plates (International Scientific, 95% transmittance) were placed in the openings of the interferometer and detector compartments. Data acquisition was triggered by a small fraction of the photolysis laser pulse detected with an EG&G Silicon photodiode (SGD-444). The same sample cell that was employed in our femtosecond experiments was used here with a peristaltic pump controlling the flow. Data were typically averaged over 15 laser-induced decays recorded for each mirror position of the step-scan apparatus, and 5−10 full time-resolved step-scan experiments were performed on each sample to ensure reproducibility and allow for statistical analysis of data. Typically, changes in optical density of 5×10^{-5} were resolvable in these experiments.

D. Density Functional Theory Calculations. DFT complexes have been deemed reliable for transition-metal complexes[5] and therefore have been used in this work to assist in the characterization of the intermediate species and to facilitate an understanding of the dynamic behavior observed. All DFT computations described herein were carried out using Gaussian03.[20] Becke's three-parameter hybrid exchange-correlation energy functional,[21] B3LYP,[22] was used in all calculations. The atomic orbital basis set used through this work consisted of the LANL2DZ core potential[23] for tungsten and the 6-311++G(d,p) basis set for all other atoms. Vibrational frequency analyses were performed on all structures to ensure that the configurations obtained correspond to minima or first-order saddle points on the potential energy surface and were used in the kinetic modeling via statistical theories for unimolecular reactions. Transition states were located using either the combined synchronous transit-guided and quasi-Newton (STQN) methods[24] or the Berny optimization algorithm.[25] All transition states were verified by following the appropriate eigenvectors, i.e., those eigenvectors associated with an imaginary frequency, to their respective interconnected stationary points.

III. Results and Discussion

The results of our time-resolved experiments are presented and discussed in the context of the DFT results and previous work in order to provide a complete picture of the rates, mechanisms, and species involved in the photochemistry of $CpW(CO)_3(CH_2CH_3)$ (**A**). This section is divided into five parts. The first part (A) describes the results of DFT studies. Multiple isomers for species **B**−**E** were found using DFT and permit multiple pathways to β-H elimination. Experimental results are described in parts B−D in the context of the various isomers established from the DFT results. Part B focuses on the primary photoproducts of **A** with an emphasis on the ultrafast results. Part C highlights the rearrangement process **B** → **D**, and part D focuses on the rearrangement **D** ↔ **E** → **F**. The last section (E) addresses the radical side reaction in which CH_2CH_3 elimination from **A** produces the radical $CpW(CO)_3^{\bullet}$. The results of this combined experiment and DFT study are summarized in Figure 8.

A. Density Functional Theory. A detailed investigation of the reaction, using DFT modeling, revealed multiple pathways to β-H elimination. A potential energy diagram (ΔG) of the various reaction pathways is shown in Figure 2, and a more complete thermodynamic comparison of the species can be found in Table 1 (see also Table S1 in the Supporting Information). The structures of the species involved in the DFT-modeled pathways are shown in Figure 3, and vibrational frequencies are given in Table 2. The reaction begins with $CpW(CO)_3(CH_2CH_3)$ (**A**). In the experimental studies discussed in the subsequent section, a single CO is photodissociated from **A**. By symmetry, there are two possible structures for the CO-loss species (**B**). If a carbonyl group located cis to the ethyl group is dissociated, the species $\mathbf{B_{cis}}$ forms, whereas when the carbonyl group located trans to the ethyl group is ejected, the species $\mathbf{B_{trans}}$ forms.

The *low-energy* path from $\mathbf{B_{cis}}$ will be discussed first followed by the pathway for the higher-energy species $\mathbf{B_{trans}}$. Previous experimental studies have suggested that the coordinatively unsaturated species (**B**) will coordinate a ligand from the solvent for additional stability.[13] On the basis of a thermodynamic comparison of the propane solvated species, $\mathbf{C_{cis,alk}}$, with unsolvated $\mathbf{B_{cis}}$, solvation with an alkane results in unfavorable changes in both the enthalpy and free energy of the complex. In the structure for $\mathbf{C_{cis,alk}}$, the solvent−metal distance (5.4 Å) is so large that the complex appears very similar to the unsolvated form,[26] $\mathbf{B_{cis}}$, indicative of a poor solvent−metal interaction. In the structure for $\mathbf{B_{cis}}$ (Figure 3) the W−H_α bond is shorter and the C_α−H_α bond is longer than the bond lengths in similar complexes (see Table S3 in the Supporting Information), indicating the presence of an agostic interaction between the α-CH and the metal. It appears that the agostic α-CH bond stabilizes $\mathbf{B_{cis}}$ to such an extent that solvent coordination is unnecessary. Such agostic M−H−C bonds are well-documented in a variety of organometallic complexes[27] and can sometimes lead to α-H elimination products.[4,6] In this study, DFT calculations indicate that α-H elimination is thermodynamically unfavorable for $\mathbf{B_{cis}}$.[28]

The path to β-H elimination begins with the formation of the bridged hydride complex $CpW(CO)_2(\mu\text{-H-}C_2H_4)$, which we have named $\mathbf{D_h}$. In this complex, the ethyl group is oriented

(19) (a) Sun, H.; Frei, H. *J. Phys. Chem. B* **1997**, *101*, 205. (b) Yeom, Y. H.; Frei, H. *J. Phys. Chem. B* **2003**, *107*, 6286.

(20) Frisch, M. J. et al. *Gaussian03*; Gaussian, Inc., Wallingford, CT, 2004.

(21) (a) Becke, A. D. *J. Chem. Phys.* **1993**, *98*, 5648. (b) Lee, C.; Yang, W.; Parr, R. G. *Phys. Rev. B* **1988**, *37*, 785.

(22) Stephens, P. J.; Devlin, G. J.; Chabalowski, C. F.; Frisch, M. M. *J. Phys. Chem.* **1994**, *98*, 11623.

(23) Hay, P. J.; Wadt, W. R. *J. Chem. Phys.* **1985**, *82*, 299.

(24) (a) Peng, C. Y.; Ayala, P. Y.; Schlegel, H. B.; Frisch, M. J. *J. Comput. Chem.* **1996**, *17*, 49. (b) Peng, C. Y.; Schlegel, H. B. *Isr. J. Chem.* **1993**, *33*, 449.

(25) Schlegel, H. B. *J. Comput. Chem.* **1982**, *3*, 214.

(26) In order to find the geometry of $\mathbf{C_{cis,alk}}$ in DFT calculations, a propane molecule was placed cis to the ethyl ligand in the complex. The DFT geometry optimization moved the propane molecule 6 Å from the metal center; however, with the generic basis set used in this study, no structure corresponding to a minimum on the potential energy surface could be identified. A lower basis set calculation (with 6-31G* for carbon, oxygen, and hydrogen atoms) resulted in the metal−solvent distance of 5.4 Å

(27) (a) Clot, E.; Eisenstein, O. *Principles and Applications of Density Functional Theory in Inorganic Chemistry II*; Springer: Berlin, Heidelberg, Germany, 2004. (b) Brookhart, M.; Green, M. L. H. *J. Organomet. Chem.* **1983**, *250*, 395.

(28) DFT calculations using a 6-31G* basis set for the non-metal atoms predict that $\mathbf{B_{cis}}$ is more stable ($\Delta H = 8.8$ kcal mol^{-1}; $\Delta G = 8.5$ kcal mol^{-1}) than the α-H eliminated complex.

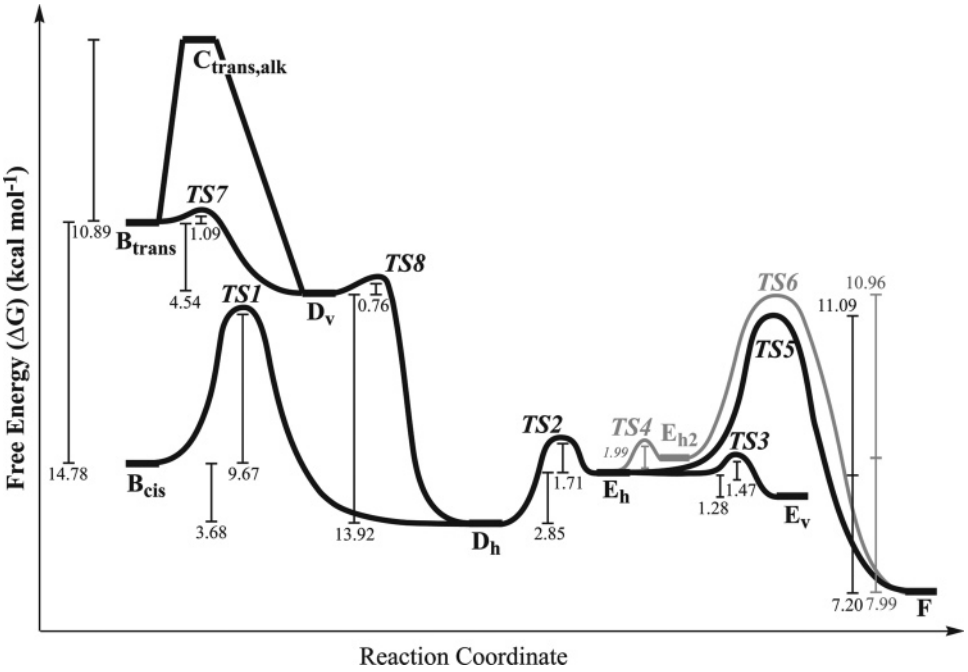

Figure 2. DFT-generated free-energy potential energy curve for all possible pathways to β-H transfer in **A**. Barrier heights and relative stabilities of all species are drawn to scale and reported in kcal mol^{-1}.

Table 1. Reaction Enthalpies/Energies and Barrier Heights for the Relevant Reactions in the Photochemistry of A

	reacn enthalpy/energy[a,b]		barrier height[a,c]	
	calcd $\Delta_r H°$	calcd $\Delta_r G°$	calcd $\Delta G^{‡o}$	exptl $\Delta G^{‡o}$
A → $\mathbf{B_{cis}}$	32.14	21.44		
$\mathbf{B_{cis}}$ → $\mathbf{C_{cis,alk}}$[d] (6-31G(d))	1.75	8.06		
$\mathbf{B_{cis}}$ → $\mathbf{C_{cis,EtOH}}$	−4.05	8.12		
$\mathbf{B_{cis}}$ → **(TS1)** → $\mathbf{D_h}$	−4.40	−3.68	9.67	10.04
$\mathbf{D_h}$ → **(TS2)** → $\mathbf{E_h}$	3.48	2.85	4.56	10.41
reverse reaction			*1.71*	*9.29*[e]
$\mathbf{E_h}$ → **(TS3)** → $\mathbf{E_v}$	−2.14	−1.34	1.47	
reverse reaction			*2.75*	
$\mathbf{E_h}$ → **(TS4)** → $\mathbf{E_{h2}}$	1.19	0.79	1.99	
reverse reaction			*1.20*	
$\mathbf{E_h}$ → **(TS5)** → **F**	−7.41	−7.20	11.09	11.09[e]
$\mathbf{E_{h2}}$ → **(TS6)** → **F**	−8.60	−7.99	10.96	
A → $\mathbf{B_{trans}}$	48.27	36.21		
$\mathbf{B_{trans}}$ → $\mathbf{C_{trans,alk}}$[d]	−0.58	10.89		
$\mathbf{B_{trans}}$ → $\mathbf{C_{trans,EtOH}}$	−14.36	−2.13		
$\mathbf{B_{trans}}$ → **(TS7)** → $\mathbf{D_v}$	−6.30	−4.54	1.09	
$\mathbf{D_v}$ → **(TS8)** → $\mathbf{D_h}$	−14.26	−13.92	0.76	
A → **radical**	34.26	19.31		

[a] In kcal mol^{-1}. Unless otherwise specified, the 6-311++G(d,p) basis set was used for nonmetal atoms; all species involved in a reaction were calculated in the same basis set. [b] Reactant enthalpy/energy is set to zero, calculated at 298 K. [c] Experimental barrier heights calculated using experimentally determined reaction rates and transition state theory ($k_{tst} = (k_b T/h) \exp(-\Delta G^{‡o}/RT)$) at $T = 298$ K. [d] Propane was used as the alkyl solvating group. [e] The experimental barrier was actually determined between an unspecified isomer of **E** and $\mathbf{D_h}$ or of **E** and **F**.

horizontally relative to the plane defined by the Cp ring, and an agostic interaction exists between the metal and the β-CH. The barrier to formation from $\mathbf{B_{cis}}$ via **TS1** is relatively high and requires rotation of the ethyl ligand from a vertical to horizontal orientation and cleavage of the $M-C_\alpha-H_\alpha$ agostic bond. As all forward barriers between $\mathbf{D_h}$ and the final product **F** are lower than the reverse reaction ($\mathbf{D_h} \rightarrow \mathbf{B_{cis}}$), it is unlikely that any significant amount of $\mathbf{B_{cis}}$ re-forms.

Species $\mathbf{D_h}$ rearranges to the β-H eliminated species $\mathbf{E_h}$ via **TS2**. This reaction has a relatively small barrier and is endothermic. In the process of β-H elimination, the $C_\beta-H_\beta$ bond lengthens by 1.14 Å and the $W-H_\beta$ bond shortens by 0.19 Å. The structure of **TS2** has been the subject of a number of previous studies. It is commonly believed that the transition-state structure comprises a four-center, nearly coplanar geometry of the α- and β-carbons, the β-hydrogen, and the metal atom.[6,12,29] A recent theoretical study demonstrated the possibility of β-H elimination in metallacycles with $M-C_\alpha-C_\beta-H_\beta$ dihedral angles far from 0°.[3] As can be seen in Table S4 in the Supporting Information, the $W-C_\alpha-C_\beta-H_\beta$ angle for **TS2** is small (12.2°) but not 0°.

Species $\mathbf{E_h}$ can rearrange over **TS3** to a slightly more stable isomer, $\mathbf{E_v}$, in which the ethylene group is oriented vertically instead of horizontally. Species $\mathbf{E_h}$ can also rearrange to a slightly less stable isomer, $\mathbf{E_{h2}}$, via a low barrier rotation of the ethylene and hydrogen ligands over **TS4**. Because the barriers for interconversion among $\mathbf{D_h}$, $\mathbf{E_h}$, $\mathbf{E_{h2}}$, and $\mathbf{E_v}$ are all quite small, the four species are expected to rapidly establish an equilibrium.

In the final step, $\mathbf{E_h}$ isomerizes to **F** via **TS5** (see Figures 2 and 3). This is the largest barrier in the reaction, making this the rate-determining step. The process of isomerization involves moving the β-H around the side of the metal to a position trans to the ethylene group. Species $\mathbf{E_{h2}}$ is also able to rearrange to species **F** over **TS6** with a barrier height that is similar to that measured for **TS5**. The isomerization process in **TS6** involves moving the β-H between the two carbonyl ligands (see Figures 2 and 3).

Many of these results are consistent with previous studies. Experimental work has established that an equilibrium exists between **D** and **E** and that the rate-determining step in the photochemistry of **A** involves rearrangement from **E** to **F**.[12,13] In addition, scrambling between α- and β-H elimination was observed previously in the product species,[12] suggesting that rotation of the ethylene group in **E** is facile. No study has established whether the coordinatively unsaturated species **B**

(29) McDermott, J. X.; White, J. F.; Whitesides, G. M. *J. Am. Chem. Soc.* **1973**, *95*, 4451.

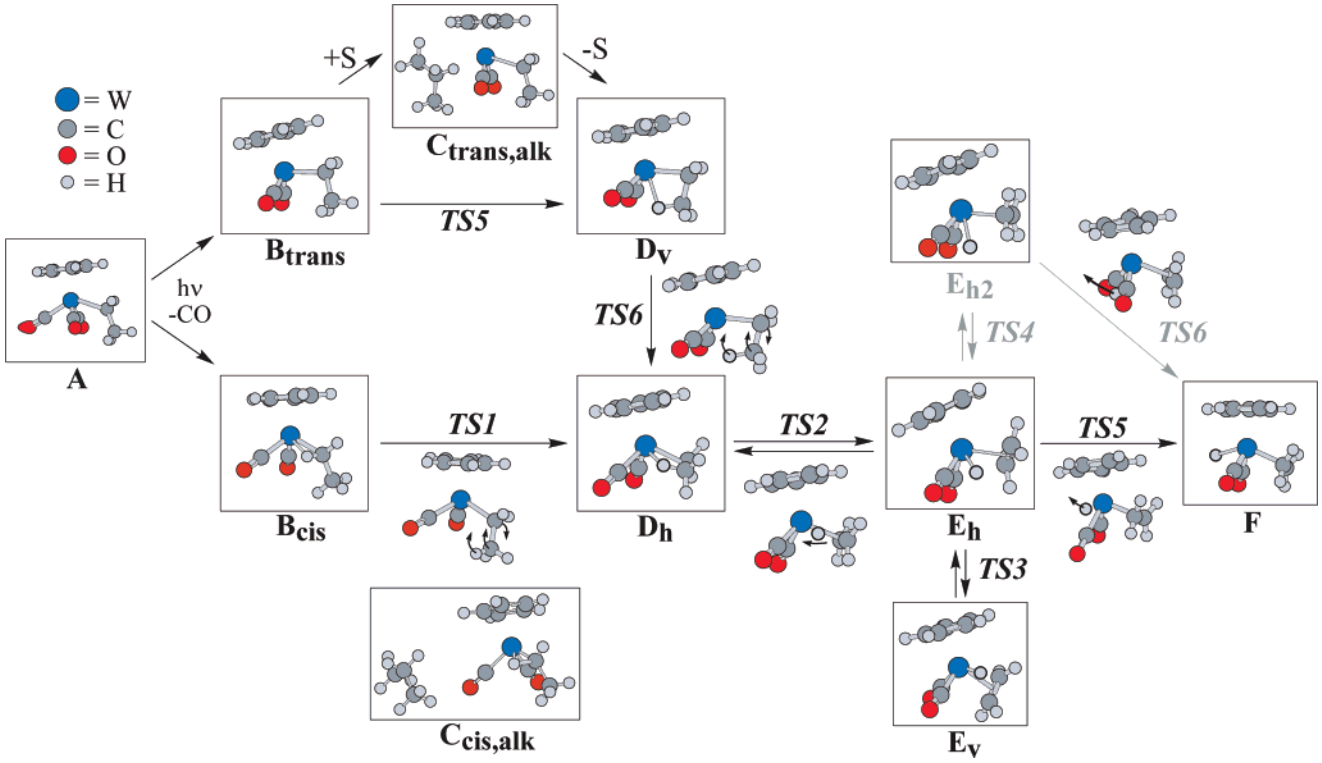

Figure 3. DFT-optimized structures of all pathways to β-H transfer in **A**. Bonds to the Cp ring are not shown, in order to better visualize the remaining ligands. $\mathbf{C_{cis,alk}}$ is not energetically favored in this reaction; it is displayed in order to illustrate the structure and metal−solvent distance.

will coordinate a molecule from an alkane solvent. On the basis of previous observations that metal hexacarbonyl complexes solvate rapidly (1−2 ps) upon dissociation of one carbonyl,[30] one might expect species **B** to solvate. Our DFT results indicate that $\mathbf{B_{cis}}$ does not form a stable solvated complex and instead stabilizes itself via an agostic α-H interaction.

The *high-energy* pathway to β-H elimination begins with dissociation of the carbonyl located trans to the ethyl ligand. $\mathbf{B_{trans}}$ is considerably less stable than $\mathbf{B_{cis}}$, possibly because $\mathbf{B_{trans}}$ is not internally stabilized via the aforementioned α-H agostic interaction.[31] Solvent stabilization and formation of $\mathbf{C_{trans,alk}}$ is enthalpically favorable, but the free energy changes are unfavorable, and it is not obvious that $\mathbf{B_{trans}}$ will solvate an alkyl group.[32] $\mathbf{B_{trans}}$ rearranges to a bridged hydride complex, $\mathbf{D_v}$, with a vertically oriented ethyl group, as shown in Figure 3. The rearrangement from $\mathbf{B_{trans}}$ to $\mathbf{D_v}$ is extremely facile and exothermic.

Once formed, $\mathbf{D_v}$ can easily rearrange, over **TS8**, to $\mathbf{D_h}$ (the same $\mathbf{D_h}$ discussed in the $\mathbf{B_{cis}}$ pathway) via rotation of the ethyl ligand (with the β-H still attached to the ethyl group). A large degree of computational effort was devoted to elucidating a direct pathway from $\mathbf{D_v}$ to $\mathbf{E_h}$ or $\mathbf{E_{h2}}$. No such pathway was found, which strongly suggests that $\mathbf{D_v}$ will rearrange exclusively to $\mathbf{D_h}$.

The results of these DFT calculations indicate the process of direct elimination, i.e., **D** → **F**, does not occur. In conclusion, all elucidated pathways required the formation of **E** ($\mathbf{E_h}$, $\mathbf{E_{h2}}$, or $\mathbf{E_v}$) via rearrangement of **D** prior to formation of **F**.

B. Ultrafast Experimental Results: Primary Photoproducts. UV photoexcitation of **A** in hexane produces a complex reaction that results in β-H elimination. Ultrafast time-resolved IR difference spectra are shown in Figure 4 with the corresponding peak assignments and kinetic fit parameters reported in Table 2. In these spectra, negative peaks (bleaches) correspond to photodepleted reactant, **A**, and positives peaks result from transients or products formed after photoexcitation.

The peak assignment for $\mathbf{A_{hot}}$, the vibrationally excited parent molecule, is based on the correlation between the decay time of $\mathbf{A_{hot}}$ and the recovery time of **A,** as well as the position of the $\mathbf{A_{hot}}$ peak on the low-frequency side of **A**.[33] A second peak assigned to $\mathbf{A_{hot}}$ is expected near ca. 2010 cm^{-1} but may be unresolvable due to its small amplitude.[34] Peaks labeled **R** are assigned, on the basis of literature values,[15] to the radical species $CpW(CO)_3^{\bullet}$ formed via dissociation of the ethyl ligand. Radical species dynamics are discussed more fully in part E. It is notable that peaks corresponding to **F** are absent from these spectra, indicating that rapid self-solvation and direct elimination (i.e., **B** → **D** → **F**) does not occur in hexane on the ultrafast time frame.[35]

(30) Dougherty, T. P.; Heilweil, E. J. *Chem. Phys. Lett.* **1994**, *227*, 19.

(31) Rearrangement from $\mathbf{B_{trans}}$ directly to $\mathbf{B_{cis}}$ is expected to have a low barrier, as the process does not involve any bond cleavage.

(32) Such a disparity between ΔH and ΔG is observed in $\mathbf{B_{cis}}$ vs $CpW(CO)_3(CH_2CH_3)(EtOH)$ ($\mathbf{C_{cis,EtOH}}$), yet our experimental results (see Figure S1 in the Supporting Information) clearly indicate that $\mathbf{C_{cis,EtOH}}$ forms despite the rise in free energy predicted by DFT. The same phenomenon has been observed with $M(CO)_5$ vs $M(CO)_5$(alkane) where M = Cr, W, Mo (unpublished DFT results); however, $M(CO)_5$(alkane) is observed to form experimentally.[30] As $\mathbf{B_{trans}}$ does not internally stabilize by forming an agostic C−H bond with the ethyl group, it seems more likely that the complex will solvate despite the DFT-predicted rise in free energy.

(33) (a) Hamm, P.; Lim, M.; Hochstrasser, R. M. *J. Chem. Phys.* **1997**, *107*, 10523. (b) Buback, M.; Kling, M.; Seidel, M. T.; Schott, F.-D.; Schroeder, J.; Steegmüller, U. *Z. Phys. Chem.* **2001**, *215*, 717. (c) Snee, P. T.; Payne, C. K.; Mebane, S. D.; Kotz, K. T.; Harris, C. B. *J. Am. Chem. Soc.* **2001**, *123*, 6909.

(34) In a related study of **A** in ethanol (see Figure S1 in the Supporting Information), two peaks assigned to $\mathbf{A_{hot}}$ were observed with similar recovery times and peak positions relative to **A**.

(35) **F** is also absent in ultrafast spectra of **A** in ethanol. See the Supporting Information.

Table 2. Peak Assignments and Dynamics from Photoexcitation of A in Hexane

species	calcd freq[a,b]/cm^{-1}	exptl freq[c]/cm^{-1}	kinetics/ps	kinetics/μs
A	1921 (0.7)	1929 (s)	20 ± 4, rise	no change
	1926 (0.4)	2020 (m)	(15% recovery)	
	2001 (0.3)			
$\mathbf{A_{hot}}$ vib excited **A**		1918 (s)	20 ± 4, decay	
$\mathbf{B_{cis}}$	1875 (0.5)	1870 (m)	23 ± 3, rise	3.7 ± 0.2, decay
	1946 (0.5)	1953 (m)		151 ± 45, decay
$\mathbf{B_{trans}}$	1857 (1.0)			
	1943 (0.3)			
$\mathbf{C_{cis,alk}}$ (6-31G(d))[d]	1897 (1.2)			
	1961 (0.9)			
$\mathbf{C_{trans,alk}}$	1865 (0.8)			
	1941 (0.2)			
$\mathbf{D_h}$	1863 (0.9)	1872 (m)		3.8 ± 0.2, decay
	1934 (0.3)	1953 (m)		150 ± 2, decay
$\mathbf{D_v}$	1878 (0.5)			
	1945 (0.5)			
$\mathbf{E_v}$	1924 (0.5)	1991 (w)[e]		7, rise
	1975 (0.5)			8, rise
				120, decay
$\mathbf{E_h}$	1883 (0.5)			
	1939 (0.5)			
$\mathbf{E_{h2}}$	1919 (0.6)			
	1967 (0.4)			
F	1904 (0.7)	1906 (m)		147 ± 2, rise
	1966 (0.4)	1981 (w)		
R	1906 (0.7)	1903 (m)	5.6 ± 0.8, rise	0.54 ± 0.06, decay
$CpW(CO)_3$	1907 (0.5)	2001 (w)		
	1989 (0.4)			

[a] Calculated frequencies are corrected by a factor of 0.9614.[52] Unless otherwise specified, the 6-311++G(d,p) basis set was used for nonmetal atoms. [b] Calculated intensities (given in parentheses) are relative to the 1957 cm^{-1} mode of $\mathbf{B_{trans}}$. [c] Observed intensities: w = weak, m = medium, s = strong. [d] Propane was used as the alkyl solvating group; for comparison purposes the frequencies of $\mathbf{B_{cis}}$ at 6-31G* are 1904 (1.0) and 1965 (1.0) and relative amplitudes are determined relative to $\mathbf{B_{trans}}$ using 6-31G*. [e] Tentative assignment.

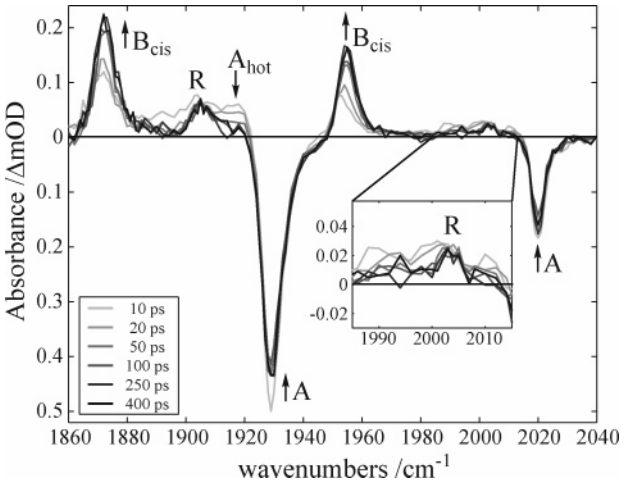

Figure 4. Spectral results with femtosecond time resolution following UV irradiation of **A** in hexane.

According to our DFT results, two different coordinatively unsaturated species may form, $\mathbf{B_{cis}}$ or $\mathbf{B_{trans}}$, and may solvate, resulting in $\mathbf{C_{cis,alk}}$ or $\mathbf{C_{trans,alk}}$. As there is sufficient energy available in the complex after excitation at 266 nm to access either $\mathbf{B_{cis}}$ or $\mathbf{B_{trans}}$, all four species must be considered for our peak assignments. DFT-predicted vibrational frequencies for all four species match the large peaks in Figure 4 (1872 and 1955 cm^{-1}) reasonably well, with $\mathbf{B_{cis}}$ showing the best match. DFT-predicted relative peak amplitudes indicate that both $\mathbf{B_{trans}}$ and $\mathbf{C_{trans,alk}}$ are a poor match with experimental peaks, as DFT predicts a large disparity in amplitude between the low- and high-frequency peaks and experimentally the peaks at 1872 and 1955 cm^{-1} have very similar amplitudes. In addition, the DFT-predicted barriers for $\mathbf{B_{trans}} \rightarrow \mathbf{D_v} \rightarrow \mathbf{D_h}$ are both so small that it is unlikely $\mathbf{B_{trans}}$ could be observed, even with ultrafast time resolution.[36] Finally, DFT calculations indicate that $\mathbf{C_{cis,alk}}$ is poorly solvated (i.e., 5.4 Å distance between the metal and solvent) and is thermodynamically less stable than $\mathbf{B_{cis}}$. The calculated vibrational frequencies of $\mathbf{B_{cis}}$ and $\mathbf{C_{cis,alk}}$ are nearly identical (Table 2), indicating a poor interaction of the alkyl with the metal. Thus, while it is impossible to state conclusively whether the peaks at 1872 and 1955 cm^{-1} result from $\mathbf{B_{cis}}$, $\mathbf{B_{trans}}$, $\mathbf{C_{cis,alk}}$, or $\mathbf{C_{trans,alk}}$, our DFT results indicate that these peaks are most likely to originate from $\mathbf{B_{cis}}$. The dynamics of the peaks exhibit changes[37] normally associated with vibrational cooling.[38]

In contrast, ultrafast studies of **A** in ethanol indicate that the species $\mathbf{B_{cis}}$ coordinates an ethanol molecule, forming $\mathbf{C_{cis,EtOH}}$ (Figure S1 in the Supporting Information) within a few picoseconds. Therefore, the tendency for $\mathbf{B_{cis}}$ to solvate depends on the solvent present and its ability to stabilize the coordinatively unsaturated complex; in the case of alkane solvents, the unsolvated species ($\mathbf{B_{cis}}$) is favored.

C. Step-Scan Experimental Results: Rearrangement from $\mathbf{B_{cis}}$ to $\mathbf{D_h}$. Nanosecond and microsecond time-resolved step-scan FTIR spectra (Figure 5) and kinetics indicate that the isomerization rate of $\mathbf{B_{cis}}$ to $\mathbf{D_h}$ is faster than that found by previous measurements. Close examination of the region between 1860 and 1880 cm^{-1} reveals two product peaks assigned, according to previous work, to **B** and **D**;[13] an enlargement of this region is presented in Figure 6a. From our DFT studies we can refine these peak assignments: the peak at 1870 cm^{-1} is most likely $\mathbf{B_{cis}}$, and the peak at 1872 cm^{-1} is $\mathbf{D_h}$.[39] Due to the considerable overlap of the two peaks, accurate

(36) $\mathbf{D_h}$ may form with a small population in the ultrafast experiments; however, most of the population of $\mathbf{D_h}$ forms on the nanosecond time frame via $\mathbf{B_{cis}}$.

(37) Peaks narrow and shift to higher frequency (i.e. blue shift) in the first ~30 ps.

(38) Dougherty, T. P.; Heilweil, E. J. *J. Chem. Phys.* **1994**, *100*, 4006.

(39) The $\mathbf{D_v}$ to $\mathbf{D_h}$ barrier is so small that $\mathbf{D_v}$ cannot be observed, if formed.

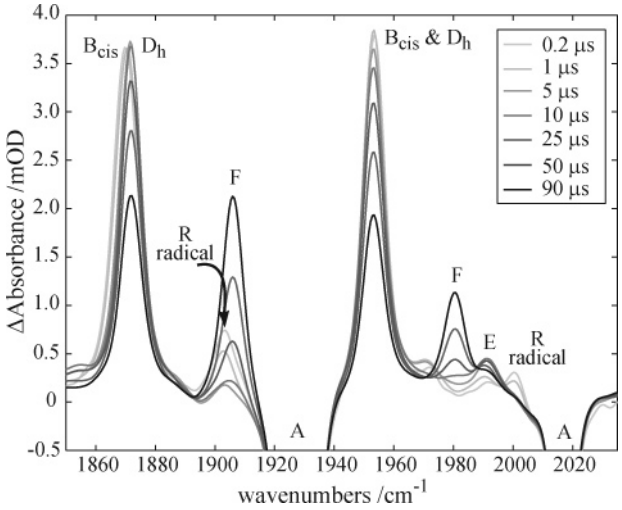

Figure 5. Spectral results with nano- and microsecond time resolution following UV irradiation of **A** in hexane. The negative peaks corresponding to **A** are not shown, in order to better visualize the product peaks.[53]

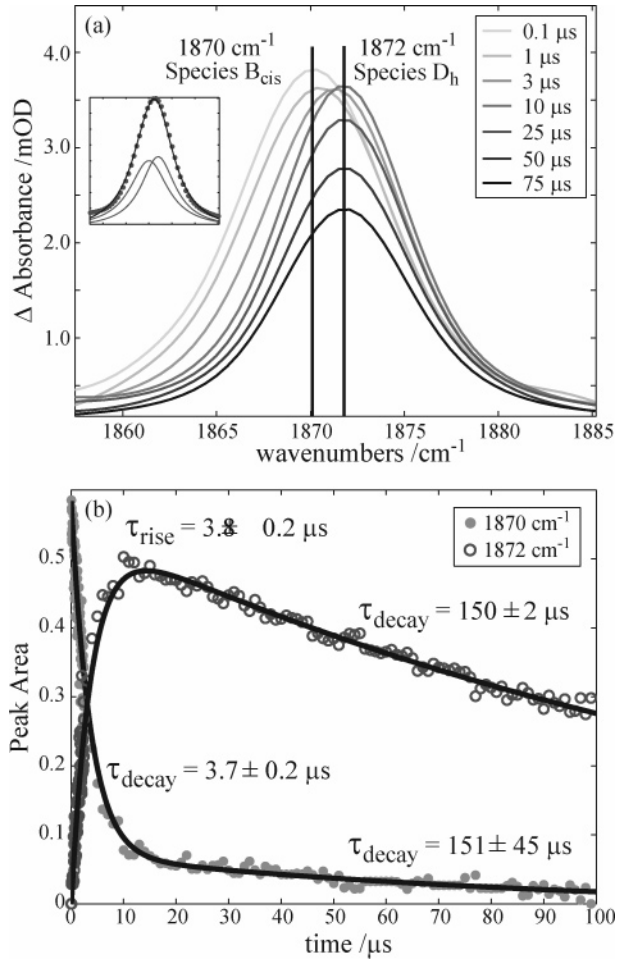

Figure 6. (a) Enlargement of the two peaks at 1870 and 1872 cm^{-1}. A representative fit at 3 μs and the contributing Lorentzians are shown in inset on the upper left. (b) Integrated peaks from (a) with fits to the data (solid lines). Corresponding time constants for formation and decay of each product are provided in the figure.

kinetics could only be obtained by fitting the spectra to two Lorentzian functions at every time slice. In this way we were able to directly measure the kinetics for the fast decay of $\mathbf{B_{cis}}$ and concomitant formation of $\mathbf{D_h}$ (Figure 6b, Table 2).[40] The

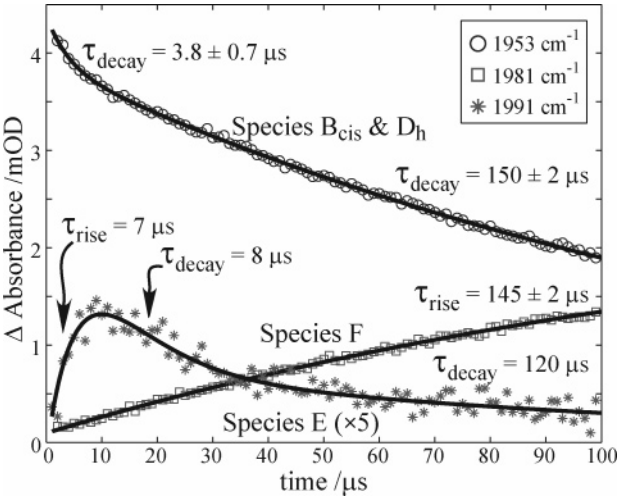

Figure 7. Peak dynamics and exponential fits for species $\mathbf{B_{cis}}$ + $\mathbf{D_h}$ at 1953 cm^{-1}, **E** at 1991 cm^{-1} (shown at 5× magnification), and **F** at 1981 cm^{-1}.

average measured rate[41] of $k_1 = (27 \pm 1) \times 10^4$ s^{-1} ($\tau_1 = 3.7 \pm 0.1$ μs) is 2−4 times larger than previous estimates;[13,14] however, we believe that the faster time resolution in our experiments (25 ns) and the method of peak fitting and integration to separate the kinetics allow for a more accurate and precise determination of the reaction rates. Remarkably, the DFT-predicted barrier to this reaction is nearly equal to the experimentally derived barrier (Table 1).

D. Step-Scan Experimental Results: Rearrangement from $\mathbf{D_h}$ to $\mathbf{E_h}$/$\mathbf{E_{h2}}$/$\mathbf{E_v}$ to F. Microsecond time-resolved step-scan FTIR experiments (Figure 5) were able to resolve the dynamics of $\mathbf{D_h}$ rearrangement to one of the isomers of **E** and subsequent rearrangement to **F**. In the spectra in Figure 5, the peak at 1991 cm^{-1}, which was previously assigned to species **E**,[11,13] could be assigned to $\mathbf{E_v}$, $\mathbf{E_h}$, or $\mathbf{E_{h2}}$. The DFT-predicted high-energy vibrational frequency for $\mathbf{E_v}$ matches the observed peak at 1991 cm^{-1} best of the three isomers, and the thermodynamic stability of $\mathbf{E_v}$ relative to $\mathbf{E_h}$ and $\mathbf{E_{h2}}$ suggests that $\mathbf{E_v}$ is the dominant species in the reaction. Due to uncertainties in the DFT-calculated reaction barriers and vibrational frequencies, this assignment remains tentative; an isomer of **E** is not specified in the forthcoming kinetic analysis.

The dynamics of species **E** at 1991 cm^{-1} show a rapid rise and biexponential decay (Table 2 and Figure 7).[42] The equilibrium constant between $\mathbf{D_h}$ and **E** was determined via the peak height ratios of $[\mathbf{E}]/[\mathbf{D_h}] = K_{eq}$ to be 0.14 ± 0.01.[43] Using these results, we calculated the experimental rates and barriers (presented in Table 1) for the individual steps in the reaction: $\mathbf{D_h} \rightarrow \mathbf{E}$, $\mathbf{E} \rightarrow \mathbf{D_h}$, and $\mathbf{E} \rightarrow \mathbf{F}$. The rate $\mathbf{D_h} \rightarrow \mathbf{E}$ (k_2 in Figure 1) was determined from the experimentally measured rate of species **E** formation, $k_2 = 14 \times 10^4$ s^{-1} (7 μs , $\Delta G^{\ddagger\circ} = 10.41$ kcal mol^{-1}). Using the relationship $K_{eq} = k_2/k_{-2}$, we estimated the reverse rate ($\mathbf{E} \rightarrow \mathbf{D_h}$) to be $k_{-2} = 96 \times 10^4$ s^{-1} ($\tau = 1$ μs;

(40) The slow decay time measured for $\mathbf{B_{cis}}$ is most likely an artifact resulting from slight mixing of kinetics that are difficult to separate due to the highly overlapped peaks or a small equilibrium between $\mathbf{B_{cis}}$ and $\mathbf{D_h}$.

(41) Experimentally derived barriers were calculated from measured reaction rates and transition state theory: $k_{tst}(T) = (k_B T/h) \exp(-\Delta G^{\ddagger\circ}/RT)$.

(42) Due to similarity of rise and decay times, errors on the fits are artificially large and a goodness of fit should be assessed by referring to Figure 7.

(43) A peak height ratio was calculated at each time between 40 and 100 μs and averaged. After 40 μs the system is assumed to be in a steady state.

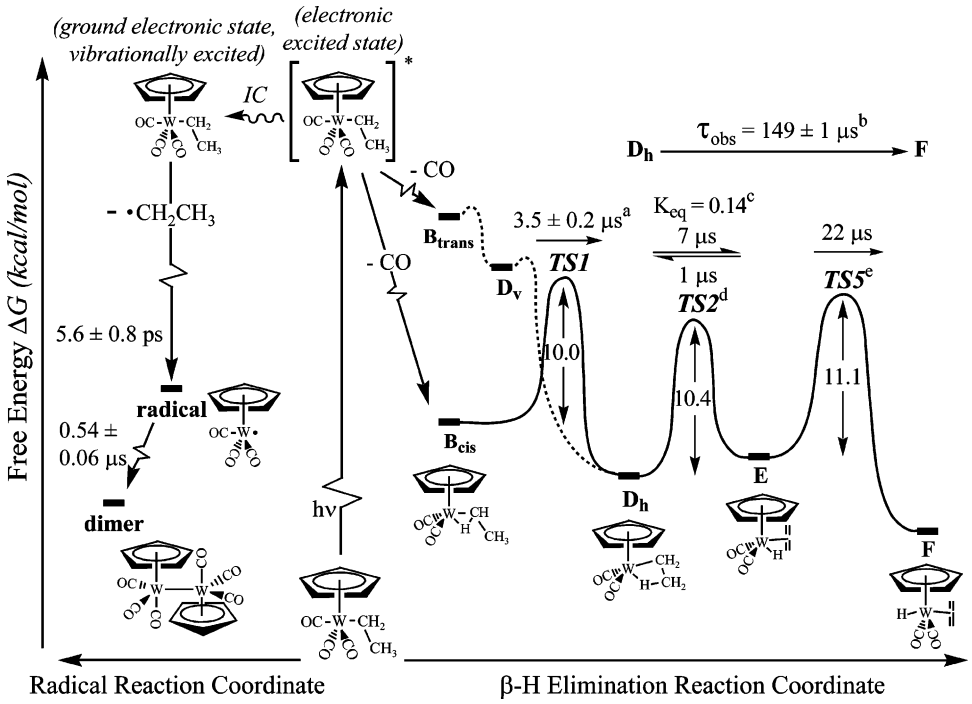

Figure 8. Principal reaction pathways and relative energetics of intermediates and transition states in the photochemistry of **A** after excitation at 266 nm. The barrier heights were determined from transition-state theory using experimentally measured rates and are reported in units of kcal mol^{-1}; the relative stabilities of the transients were obtained from DFT calculations, as listed in Table 1, and drawn to scale in units of kcal mol^{-1}.

$\Delta G^{\ddagger\circ} = 9.29$ kcal mol^{-1}). Finally, the rate constant for **E** → **F** was determined using the relationship $k_3 = k_{obs}/K_{eq}$ to be $k_3 = 4.6 \times 10^4$ s^{-1} ($\tau = 22$ μs; $\Delta G^{\ddagger\circ} = 11.09$ kcal mol^{-1}).[44] It is clear that k_3 is the rate-determining step in the β-H elimination reaction (**A** → **F**), as demonstrated in a previous study.[12] It is interesting to notice that in the kinetics of **E** there is a fast decay followed by a slow decay. The slow decay ($\tau = 120$ μs) is attributed to equilibration and slow formation of species **F**. The fast decay has not been observed previously and is tentatively assigned to another route for the formation of **E** (possibly a small population from $\mathbf{B_{trans}}$) that requires equilibration with $\mathbf{D_h}$ on this time scale.

Qualitatively, DFT predictions for the thermodynamic relationships between species $\mathbf{D_h}$ and $\mathbf{E_v}$ exhibit excellent agreement with experimental observations. For example, the equilibrium constant (K_{eq}) between species $\mathbf{D_h}$ and $\mathbf{E_v}$ was estimated from our DFT calculations via[45]

$$K_{eq}(T) = \frac{Q_{vib}{}^{E} Q_{rot}{}^{E}}{Q_{vib}{}^{D} Q_{rot}{}^{D}} \exp\left(-\frac{\Delta E_0}{RT}\right) \qquad (1)$$

where ΔE_0 denotes the zero-point energy corrected difference between $\mathbf{D_h}$ and $\mathbf{E_v}$, and Q^D and Q^E denote the vibrational and rotational partition functions of $\mathbf{D_h}$ and $\mathbf{E_v}$, respectively. The calculated K_{eq} value of 0.02 ($T = 298$ K) is less than our experimental K_{eq} value, yet both indicate that the equilibrium favors $\mathbf{D_h}$ (this can also be seen in the thermodynamic stability of $\mathbf{D_h}$ vs $\mathbf{E_v}$ in Figure 2).[46]

Quantitatively, DFT underestimates the reaction barrier for $\mathbf{D_h}$ over **TS2** relative to our experimental determination. The experimental barrier height is in good agreement with an earlier estimate.[12] The disparity in the barrier heights of our experiment and DFT predictions is most likely due to the approximations inherent to finite basis DFT computations, which often result in small differences between experimental and calculated energetics.[47]

In the final reaction, $\mathbf{E_h}/\mathbf{E_{h2}}/\mathbf{E_v}$ → **F**, DFT and experiment are consistent, both qualitatively and quantitatively. The predicted reaction barrier over **TS5** (or **TS6**) is equivalent to (or slightly smaller than) the experimental barrier (Table 1).[48] In addition, both the predicted and experimental barriers are larger than any other reaction barrier, making this final step rate determining (see Table 1).

E. Radical Side Reaction. The side reaction for **A** involves dissociation of the ethyl ligand, resulting in the radical CpW(CO)$_3$•. In the ultrafast results two peaks were observed and assigned to the radical (Table 2 and Figure 4) on the basis of previous assignments.[15] The formation time for the radical species (Table 2, and Figure S4 in the Supporting Information) indicates that this species may originate from a vibrationally hot parent molecule ($\mathbf{A_{hot}}$) rather than an excited-state complex. If ethyl dissociation resulted from the excited state, one would expect the process to be rapid (~100 fs), as it is with CO dissociation.[49]

Our measurement of the radical decay time (Table 2) is consistent with an existing study in which the radical peak was only observed in the first microsecond after photoexcitation.[15] Studies by these authors at longer delay times indicate that the radical decay pathway results in the formation of [CpW-

(44) k_{obs} is the average of the decay time of $\mathbf{D_h}$ and the rise time of **F**.

(45) Steinfeld, J. I.; Francisco, J. S.; Hase, W. L. *Chemical Kinetics and Dynamics*; Prentice Hall: Upper Saddle River, NJ, 1999.

(46) $\mathbf{E_v}$ is described because it is the most stable of the three isomers of **E**. The K_{eq} value for $\mathbf{E_h}$ and $\mathbf{D_h}$ is 0.001, and the K_{eq} value for $\mathbf{E_{h2}}$ and $\mathbf{D_h}$ is 0.0001. All K_{eq} values demonstrate that the equilibrium favors $\mathbf{D_h}$.

(47) Thomas, J. L. C.; Hall, M. B. *Organometallics* **1997**, *16*, 2318.

(48) The experimental barrier was actually determined between $\mathbf{E_v}$ and **F**; however, the rearrangement barrier from $\mathbf{E_v}$ to $\mathbf{E_h}$ is so low that our estimated barrier is expected to be only a slight overestimate of the true barrier.

(49) Lian, T.; Bromberg, S. E.; Asplund, M. C.; Yang, H.; Harris, C. B. *J. Phys. Chem.* **1996**, *100*, 11994.

$(CO)_3]_2$;[15] we found a small peak between 1960 and 1980 cm^{-1} (Figure 4), indicating that a dimer forms in our experiments as well. The dynamics of this process are, however, obscured by overlapping bands of the β-H elimination pathway, and we cannot comment further on the formation of $[CpW(CO)_3]_2$, whose photochemistry was investigated by our group in independent studies.[50]

IV. Summary

The photochemistry of $CpW(CO)_3(CH_2CH_3)$ (**A**), a prototypical transition-metal alkyl complex, was studied using ultrafast infrared and step-scan FTIR spectroscopy combined with DFT modeling. For the first time we were able to address all β-H elimination pathways as well as possible side reactions. Figure 8 summarizes our findings on the photochemistry of **A**.

Using ultrafast infrared spectroscopy, we were able to determine the formation mechanism for the radical species $CpW(CO)_3^{\bullet}$. From our ultrafast results it is also clear that the direct elimination reaction (**D** → **F**) does not occur. Our DFT results indicate the direct elimination reaction is unfeasible and an isomer of the β-H eliminated species **E** always forms from one of the **D** isomers. DFT also allowed for a proper assignment of **B**, discrediting a previous supposition that the CO-loss complex is likely to solvate a token alkane solvent molecule.[13] Using step-scan infrared spectroscopy, we were able to determine the dynamics of species **E** for the first time, allowing for a complete analysis of the barriers and kinetics of each step in the reaction. Finally, using DFT we were able to resolve the structures of each transient species involved in the photochemistry of species **A**. As species **A** is a model metal−alkyl complex,[12,13,51] many of these results can be applied to reactions of similar complexes in which the metal, alkyl chain length, and spectator ligands vary.[4,6]

Acknowledgment. The National Science Foundation is acknowledged for funding, and the Office of Basic Energy Sciences, Chemical Sciences Division, of the U.S. Department of Energy under Contract DE-AC02-05CH11231 is acknowledged for the use of some specialized equipment. Heinz Frei is acknowledged for the use of his step-scan FTIR apparatus. We thank Karl Tupper for his help with the synthesis of the starting material. M.F.K. acknowledges support by the Alexander von Humboldt Foundation through a Feodor-Lynen Fellowship. Karma Sawyer, Jacob Schlegel, James Cahoon, and Steve Shipman are acknowledged for helpful discussions.

Supporting Information Available: Text giving results and discussion pertaining to the photochemistry of $CpW(CO)_3(CH_2CH_3)$ in ethanol, figures giving DFT structures of $\mathbf{C_{cis,EtOH}}$ and $\mathbf{C_{trans,EtOH}}$, kinetics of radical $CpW(CO)_3^{\bullet}$ formation, and an expanded view of step-scan spectra between 1895 and 1915 cm^{-1}, and tables giving energies/enthalpies of individual species relative to $\mathbf{B_{cis}}$, DFT-calculated bond lengths and angles of all relevant species in the photochemistry of $CpW(CO)_3(CH_2CH_3)$, and coordinates, calculated frequencies, and raw energies for every DFT-calculated species and transition state. This material is available free of charge via the Internet at http://pubs.acs.org.

OM060455I

(50) (a) Kling, M. F.; Cahoon, J. F.; Glascoe, E. A.; Shanoski, J. E.; Harris, C. B. *J. Am. Chem. Soc.* **2004**, *126*, 11414. (b) Cahoon, J. F.; Kling, M. F.; Schmatz, S.; Harris, C. B. *J. Am. Chem. Soc.* **2005**, *127*, 12555.

(51) Kazlauskas, R. J.; Wrighton, M. S. *Organometallics* **1982**, *1*, 602.

(52) Scott, A. P.; Radom, L. *J. Phys. Chem.* **1996**, *100*, 16502.

(53) Note that slight differences in absolute peak positions between the picosecond and the nano-/microsecond data originate from the use of two completely independent experimental setups. This does not affect the determination of the kinetics of the transient species.

(54) (a) Simon, J. D.; Xie, X. *J. Phys. Chem.* **1987**, *91*, 5538. (a) Simon, J. D.; Xie, X. *J. Phys. Chem.* **1986**, *90*, 6751. (b) Joly, A. G.; Nelson, K. A. *J. Phys. Chem.* **1989**, *93*, 2876. (c) Joly, A. G.; Nelson, K. A. *Chem. Phys.* **1991**, *152*, 69.

(55) The correction factor was determined by minimizing the deviation from experimentally obtained frequencies in hexane solutions.